How to cite: *Angew. Chem. Int. Ed.* **2023**, *62*, e202218679
doi.org/10.1002/anie.202218679

Porous Salts

Porous Salts Containing Cationic Al_{24}-Hydroxide-Acetate Clusters from Scalable, Green and Aqueous Synthesis Routes

Bastian Achenbach, Erik Svensson Grape, Mohammad Wahiduzzaman, Sandra K. Pappler, Marcel Meinhart, Renée Siegel, Guillaume Maurin, Jürgen Senker,* A. Ken Inge,* and Norbert Stock**

Abstract: The solution chemistry of aluminum is highly complex and various polyoxocations are known. Here we report on the facile synthesis of a cationic Al_{24} cluster that forms porous salts of composition $[Al_{24}(OH)_{56}(CH_3COO)_{12}]X_4$, denoted CAU-55-X, with $X = Cl^-$, Br^-, I^-, HSO_4^-. Three-dimensional electron diffraction was employed to determine the crystal structures. Various robust and mild synthesis routes for the chloride salt $[Al_{24}(OH)_{56}(CH_3COO)_{12}]Cl_4$ in water were established resulting in high yields (>95 %, 215 g per batch) within minutes. Specific surface areas and H_2O capacities with maximum values of up to 930 $m^2 g^{-1}$ and 430 $mg g^{-1}$ are observed. The particle size of CAU-55-X can be tuned between 140 nm and 1250 nm, permitting its synthesis as stable dispersions or as highly crystalline powders. The positive surface charge of the particles, allow fast and effective adsorption of anionic dye molecules and adsorption of poly- and perfluoroalkyl substances (PFAS).

Introduction

Aluminum is the third most abundant element in the earth's crust at 8.2 percent by weight and its compounds are of great economic importance. It is employed as a metal due to its low density and high electrical conductivity. This chemical element is found in oxides/hydroxides such as corundum,[1–3] alumina, zeolites,[4] AlPOs[5–7] and LDH's[8,9] which are used as catalyst supports,[10] abrasives[11] or fillers.[12,13] The chemistry of Al^{3+} ions in aqueous solution is very complex and has been intensively studied. It is characterized by its amphoteric character, condensation reactions and the formation of polyoxocations.[14–17] The best-known examples are the Al_{13} Keggin ions of composition $[AlO_4Al_{12}(OH)_{24}(OH_2)_{12}]^{7+}$[18,19] and the Al_{30} cluster.[16] In addition, Al-O-clusters containing carboxylate groups have been described, many of which are also known as inorganic building units in metal–organic frameworks (MOFs).[20–23]

Porous molecular cages, including metal organic polyhedra, metal complexes, porous organic salts or organic molecules of intrinsic microporosity, have attracted substantial attention since they allow tuning host-guest interactions.[24–27] Salts containing charged porous coordination cages have been reported where counter ions are used to control material properties.[28–30]

In the present study, we describe the discovery, synthesis optimization and characterization of a series of porous aluminum salts $[Al_{24}(OH)_{56}(CH_3COO)_{12}]X_4$ denoted as CAU-55-X, containing a cationic Al_{24} cluster. Unlike existing Al-based porous crystalline compounds such as zeolites, AlPOs and MOFs, the porosity in CAU-55 is due to the assembly of porous cationic cages with anions, resulting in intra- and inter-cage porosity. It's discovery is very surprising as aluminum acetates have been studied and used industrially for more than 100 years.[31–36] In addition, CAU-55 is obtained under mild reaction conditions from common starting materials. For example, the reaction of sodium acetate with an aluminum salt in water at room temperature already results in the formation of CAU-55.

Various synthesis procedures were established and the most flexible protocol involves $NaAlO_2$, CH_3COOH and

[*] B. Achenbach, Prof. Dr. N. Stock
Institute of Inorganic Chemistry, Kiel University
Max-Eyth-Str. 2, 24118 Kiel (Germany)
E-mail: stock@ac.uni-kiel.de
E. S. Grape, Dr. A. K. Inge
Department of Materials and Environmental Chemistry, Stockholm University
Stockholm (Sweden)
E-mail: andrew.inge@mmk.su.se
Dr. M. Wahiduzzaman, Prof. Dr. G. Maurin
ICGM, Université Montpellier, CNRS, ENSCM
34293 Montpellier (France)
E-mail: guillaume.maurin1@umontpellier.fr
S. K. Pappler, M. Meinhart, Dr. R. Siegel, Prof. Dr. J. Senker
Inorganic Chemistry III and Northern Bavarian NMR Centre, University of Bayreuth
Universitätsstrasse 30, 95440 Bayreuth (Germany)
E-mail: juergen.senker@uni-bayreuth.de
Prof. Dr. N. Stock
Kiel Nano, Surface and Interface Science KiNSIS, Kiel University
Christian-Albrechts-Platz 4, 24118 Kiel (Germany)

NaX, which allows the incorporation of different counter ions (X^-).

Results and Discussion

Synthesis

The investigation of the chemical system $AlCl_3/CH_3COOH/NaOH$ was carried out in our custom made 2 mL high-throughput reactors[37] by systematically varying the molar ratios between 0.5–4 (Al^{3+}), 3–9 (CH_3COOH) and 3–9 (NaOH) equivalents, respectively (one equivalent corresponds to 0.18 mmol). The reaction temperature was varied between 70–130 °C (Figure 1a; Table S1.1). The formation of CAU-55-Cl is observed under a wide variety of conditions when equimolar amounts of NaOH and CH_3COOH are used. Larger deviation from a 1:1 ratio results in the formation of different polymorphs of $AlO_x(OH)_y$ or $Al(OH)(CH_3COO)_2$. The optimized reaction conditions $AlCl_3/CH_3COOH/NaOH = 1:5:5$ were used to further investigate the influence of reaction time and temperature.[38]

While CAU-55-Cl can be formed at room temperature within 28 days, full crystallization is accomplished much faster at higher reaction temperatures, and in situ PXRD studies showed that full crystallization is achieved within 3, 10 and 20 minutes at reaction temperatures of 100, 90 and 80 °C, respectively (Figure 1b; Figure S1.1.1–Figure S1.1.4). In situ ^{27}Al NMR spectroscopy at 70 °C shows a fast decrease in the concentration of Al^{3+} ions and the formation of a solid (Figure 1c; Figure S2.2.1–Figure S2.2.2).

The incorporation of other counter ions is easily accomplished under similar reaction conditions employing equimolar amounts of NaOH and CH_3COOH, but varying the aluminum salt. Thus variation of the aluminum salt to $Al_2(SO_4)_3$ (Table S1.2) resulted in the formation of CAU-55-HSO_4, while the route employing $NaAlO_2$, CH_3COOH and NaX, in a molar ratio of 1:4:1, is more versatile and allows the incorporation of the counter ions Cl^-, Br^-, I^- and HSO_4^- (Figure 2; Table S1.3). According to equation 1, a large amount of CH_3COOH and NaX, are necessary for the formation of CAU-55.[38]

$$24\,NaAlO_2 + 12\,CH_3COOH + 4\,NaX + 36\,H_2O \rightarrow [Al_{24}(OH)_{56}(CH_3COO)_{12}]X_4 + 28\,NaOH \quad (1)$$

Synthesis scale up of CAU-55-Cl was also carried out increasing the size of the batch reactor step-wise by an overall factor of 10000, i.e. from 1 ml (22 mg) to 10 L (215 g). In addition, continuous synthesis was accomplished

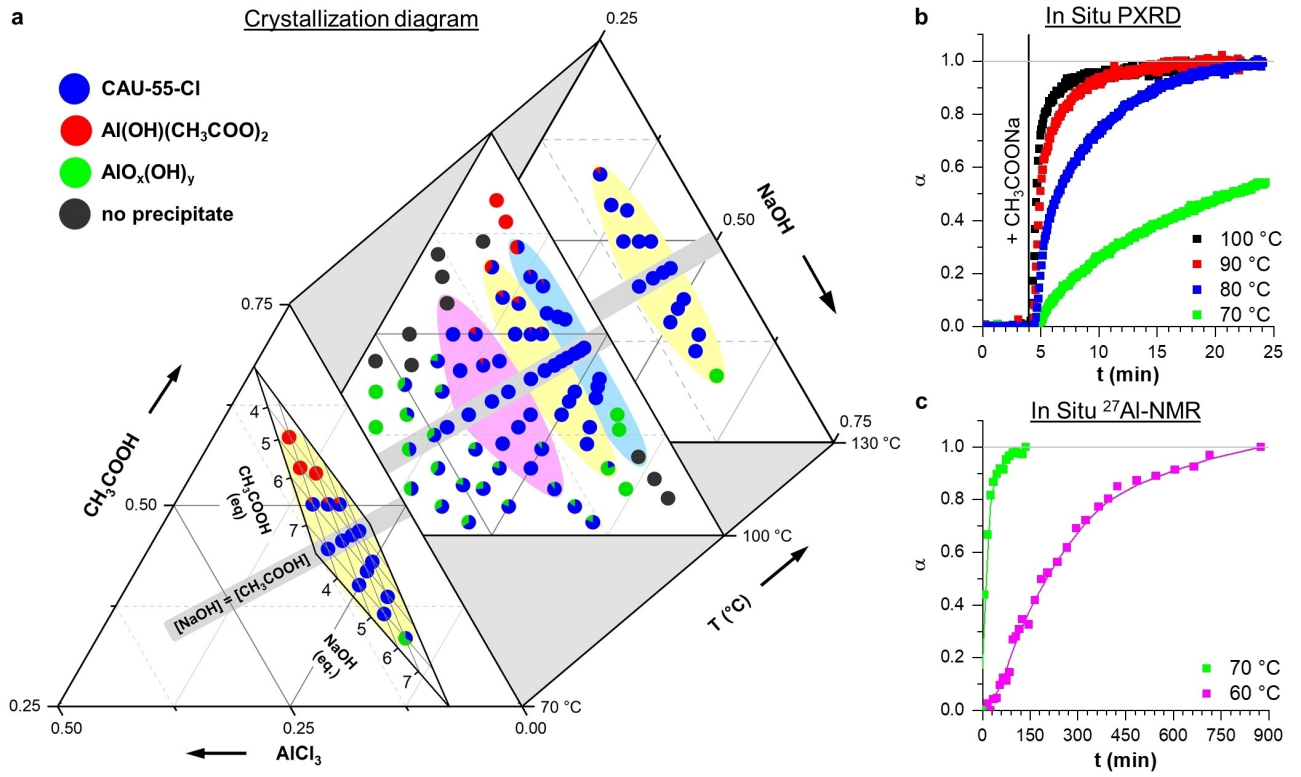

Figure 1. a) Crystallization diagrams of observed phases in the chemical system $AlCl_3/CH_3COOH/NaOH$ for reactions carried out at 70, 100 and 130 °C using high-throughput methods. The phases that are formed are color-coded and the presence of phase mixtures are presented by pie charts. Blue, yellow and magenta colored regions correspond to 0.5, 1 and 2 equivalents of $AlCl_3$ in the reaction mixture, respectively. b) Plot of extent of crystallization (α) as a function of time for in situ PXRD experiments performed at 70 °C (green), 80 °C (blue), 90 °C (red) and 100 °C (black). The vertical black line marks the time (4 min) at which the sodium acetate (NaO_2CCH_3) solution was added. c) Plot of extent of crystallization (α) determined by the decrease in the concentration of Al^{3+} ions in solution as a function of time for in situ ^{27}Al NMR experiments performed at 60 °C (pink) and 70 °C (green).

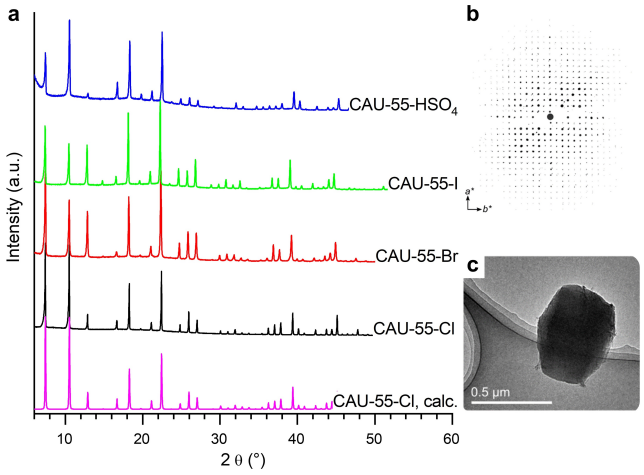

Figure 2. a) PXRD pattern of CAU-55 compounds with different counter ions. b) Reconstructed reciprocal space projection of CAU-55-Cl from the collected 3D ED data and c) transmission electron microscopy image of the crystal from which the 3D ED data were collected.

in a flow reactor (Figure S1.1f) with a residence time of 5 min in the reactor with a space-time yield of STY = 87 $kg\,h^{-1}\,m^{-3}$. For batch reactor and flow reactor syntheses the same compositions and concentrations of reactants can be used. This demonstrates the robustness of the synthesis conditions, which tolerates even various anions (Table S1.2–Table S1.5). Therefore, a versatile, green synthesis procedure was developed, using cheap, readily available and environmentally benign starting materials. The short reaction time, mild synthesis conditions and the scalability are also important factors for possible practical applications.

Crystal Structure

The CAU-55 materials were obtained as nano to microcrystalline products (Figure 3) and for some of them (X = Cl, Br, I) structure determination was carried out by three-dimensional electron diffraction (3D ED) followed by Rietveld refinement against X-ray diffraction data for CAU-55-Cl and further confirmed by Density Functional Theory

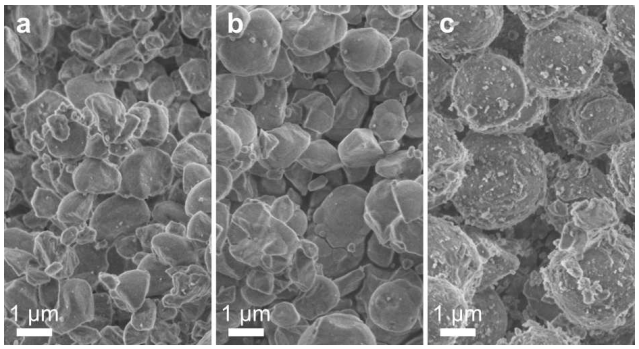

Figure 3. Scanning electron micrographs of a) CAU-55-Cl, b) CAU-55-Br, and c) CAU-55-I acquired at 10000 times magnification.

(DFT) geometry optimization (see ESI). The 3D ED method provides single crystal data on (sub)micrometer sized single crystals.. Le Bail fits were carried out for CAU-55-Br, -I and -HSO_4 to confirm phase purity and to determine the lattice parameters (Figure S3.1.1–Figure S3.1.4; Table S3.1 and Table S3.2). In the following, the structure of CAU-55-Cl (Figure 4) is described.[39] The compound crystallizes in the highly symmetric space group *Im*-3*m* (no. 229) and contains $[Al_{24}(OH)_{56}(CH_3COO)_{12}]^{4+}$ ions, also denoted as Al_{24} ions. They are composed of well-known $\{Al_3(\mu_3\text{-}OH)(\mu_2\text{-}OH)_3\}^{5+}$ trinuclear building units. These are also observed, for example, in Al_{13} Keggin ions[18,19] and are similar to the ones in the Al-MOFs MIL-96,[40,41] -100[42,43] and -101.[44,45] In the two latter MOFs the trinuclear units are connected through the carboxylate groups to give supertetrahedra which form the framework. In Al_{13} and Al_{24}, edge sharing of adjacent trinuclear unit through μ-OH-groups is observed leading to higher degrees of condensation. The structure of Al_{13} and Al_{24} can be formally derived from the assembly of four and eight trinuclear clusters into a tetrahedron and a cube respectively. Truncation of the polyhedra and occupation of the newly formed faces by the trinuclear ions followed by their interconnection through the μ-OH groups leads to the cage structures. In the case of Al_{13} the structure is related to an octahedron with 4 of the 8 triangular faces occupied by the trinuclear clusters, and the other four faces parallel to the pore window. In the case of Al_{13} an additional Al^{3+} ion is incorporated at the tetrahedral center. In Al_{24} adjacent trinuclear clusters are further interconnected by acetate ions. The structure of the Al_{24} ion is related to a cuboctahedron, with the 8 triangular faces occupied by the trinuclear cluster, the 6 square faces parallel to the pore windows and the 12 vertices occupied by the acetate ions. The inner diameter of the Al_{24} cage amounts to ≈3.8 Å (Figure S3.5.1). Similar clusters have been very recently reported which contain methoxy or ethoxy groups partially replacing the OH groups and more complex organic ligands. In addition, these compounds were synthesized in much lower yields (< 50 %) employing organic solvents and long reaction times.[46,47] In the crystal structure of CAU-55-X, a body-centered cubic packing of the Al_{24} ions, with counter ions partially occupying the octahedral voids. However, due to favorable interactions with the μ-OH sites on the cage windows, a shift of Cl^- ions from the ideal position ($^1/_2$ 0 $^1/_2$ and $^1/_2$ 0 0) to ($^1/_2$ *y* $^1/_2$ and *x* 0 0) towards the windows is found. Indeed, the DFT-optimized structure confirms that the Cl^- ions are located on the apex of equilateral square pyramids with four H(μ-OH) atoms on the base (Figure 4d) with a characteristic distance between Cl^- and H(μ-OH) of 2.19 Å (Figure S3.4.1).

Characterization

All compounds were thoroughly characterized in terms of composition as well as thermal, sorption and colloidal properties. EDX analyses were carried out to determine the Al to X ratio (Table S4.2).

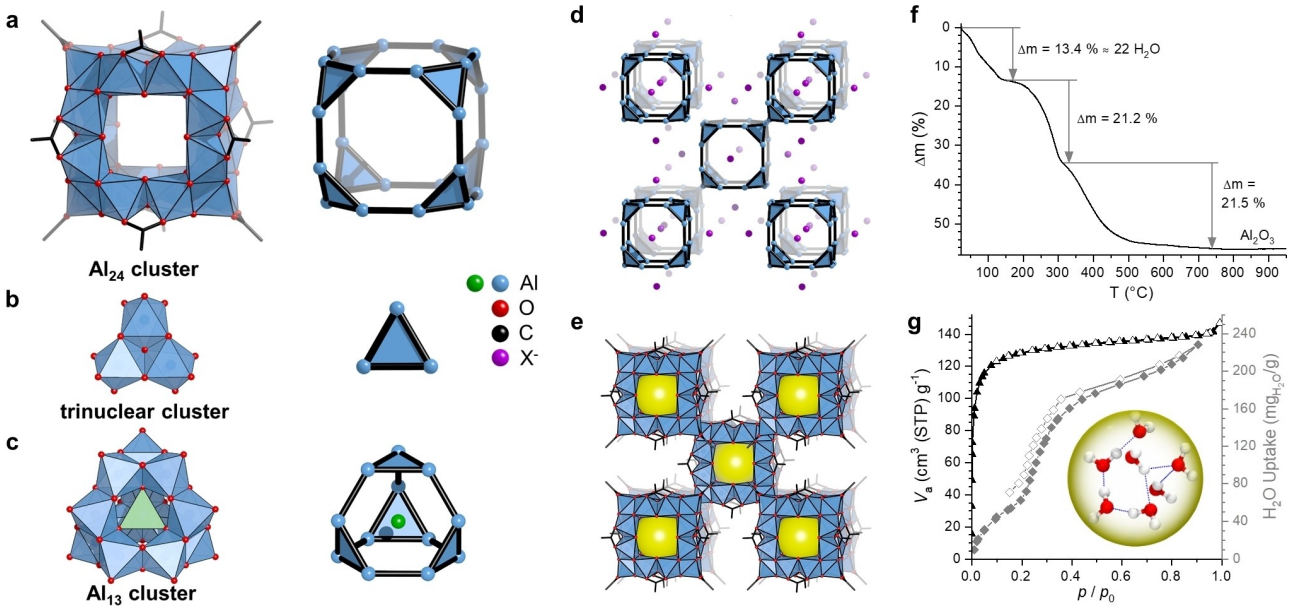

Figure 4. Crystal structure of CAU-55. a)–(c) structural relationship between the Al_{24} cluster ion $\{[Al_{24}(OH)_{56}(CH_3COO)_{12}]^{4+}\}$ (a) built up from trimeric building units (b) compared to the Keggin ion (c). d) and e) Body centered packing of Al_{24} cluster cations and anions ($X^- = Cl^-$, Br^-, I^-, HSO_4^-) occupying the octahedral voids, the cages being marked by yellow spheres. f) Thermogravimetric curve and decomposition steps of CAU-55-Cl measured with a heating rate of 4 K/min in air atmosphere allowing the determination of the water content of the sample. g) N_2 sorption (black triangles) and H_2O sorption (grey squares) isotherm of CAU-55-Cl collected at 77 K and 298 K, respectively, and distribution of the water molecules in the Al_{24} cage (yellow sphere) revealed by Monte Carlo (MC) simulations performed with 22 H_2O molecules per formula unit.

In addition to aluminum and the counter ions, Na was also detected in most of the samples. The theoretical molar ratio of Al:X = 24:4 is observed in many cases, but it can deviate substantially, with a strong dependence on the counter ion. Smaller ratios, i.e., an excess of the counter ion, are only observed for $X = Cl^-$ in conjunction with additional Na^+ ions to compensate the overall electronic charge of the system. Excessive washing of the sample does not lead to changes of the composition and, therefore, the ions must be trapped in the pores. Electron density within and between the cages was observed which could be due to water molecules or sodium ions. A special case is CAU-55-HSO_4. EDX analysis revealed a molar ratio Al:S:Na of 24:3.6:1.5. Taking the large amounts of Na^+ ions into account, which could not be removed by washing, the presence of SO_4^{2-} ions seems likely. Elemental analysis (Table S6.1) in combination with thermogravimetric measurements (Figure 4f; Figure S5.1–S5.4) allows the determination of the water content and the composition of the samples (Table S6.2). Depending on the counter ion, removal of the water molecules is found at different temperatures (room temperature to approximately 200 °C) and in some cases well-defined plateaus and weight loss steps are observed. In the following, only the data for CAU-55-Cl is presented, the other data are available in the Supporting Information. Up to 180 °C, the 22 water molecules per formula unit are desorbed. Further heating to 900 °C leads to a reaction product of low crystallinity, which can be assigned to Al_2O_3.

Monte Carlo (MC) simulations were performed at this water loading to gain insight into the distribution of water molecules in CAU-55-Cl (Figure 4g). The results show that each cage can accommodate 5 to 7 water molecules (Figure 4i) and the remaining ones are located in the inter-cage voids. This observation holds true regardless of whether Cl^- ions are fixed at their initial DFT-optimized positions or are allowed to move upon water loading during the MC simulations (Figures S3.6.1 and S3.6.2).

IR spectroscopy of CAU-55-X confirms the presence of carboxylate and sulfate ions and the water content of the samples correlates with the intensity of the broad band in the region 3000–3700 cm^{-1} (Figure S4.1; Table S4.1).

Using the information from the TG measurements, the samples were activated under reduced pressure to remove the guest molecules. Long-range order of the samples after the sorption measurements were confirmed by PXRD (Figure S7.1.4–S7.1.7) and removal of water molecules result in a reduction of the lattice parameters, i.e. a smaller unit cell, and variations of the relative intensities of the reflections (Figure S3.3.1–S3.3.2). N_2 at 77 K, H_2O sorption measurements at 298 K and ^{129}Xe NMR spectroscopic experiments using hyperpolarized ^{129}Xe[48] at variable temperatures were carried out to confirm the porosity of CAU-55 compounds (Figure 4g; Figure S7.1.1–Figure S7.1.3; Figure S7.2.1). The N_2 sorption isotherm of CAU-55-Cl shows a Type I shape up to $p/p_0 \approx 0.1$, while for H_2O an S-shape ($0.1 < p/p_0 < 0.45$) is found. Only a small hysteresis is observed in the latter sorption isotherms. Evaluation of the N_2 sorption data results in a BET surface area of $s_{BET} = 490\ m^2 g^{-1}$ and a micropore volume of $0.216\ cm^3 g^{-1}$ in line with the theoretical pore volume assessed from the DFT-optimized structure ($0.20\ cm^3 g^{-1}$). A 3D PSD map of CAU-55-Cl presented in Figure S3.5.2 evidences that, in addition to the Al_{24} cages,

significant porosity arise from the intercage voids. MC simulations were carried out to elucidate the plausible distribution of experimentally determined adsorbed N_2 molecules within the pore space of CAU-55-Cl (Figure S3.6.3 and S3.6.4). Indeed, we found that N_2 molecules are distributed within the intercage voids and inside the Al_{24} cages. ^{129}Xe NMR spectroscopic measurements further confirm that both pores, i.e. the ones within the Al_{24} clusters and the void space between the clusters can be assessed, which in turn confirms the flexibility of the cage windows (Figure S7.2.1). It is worth noting that CAU-55-Cl also exhibits a relatively large water uptake of 320 mg g^{-1} at $p/p_0 = 0.9$ (Figure 4g).

The isotherms of the other CAU-55 samples exhibit a very similar shape but specific surface areas ($350 < s_{BET} < 930\ m^2 g^{-1}$) and maximum water sorption capacities ($140 < H_2O$ uptake < 430 mg g^{-1}) vary strongly. These data are presented in Table S7.1.1. Hysteresis is prominent in some of the water sorption measurements.

The particle size of CAU-55-X samples depend on the counter ions, the Al^{3+} concentration and the reaction temperature employed and range from 140 to 1250 nm (Table S8.1). Systematic studies were carried out for CAU-55-Cl. The smallest particle sizes (≥ 140 nm) were found at low reaction temperatures, high overall concentrations, and a molar ratio of $CH_3COOH:NaOH < 1$, while the largest particles (≤ 250 nm) were observed employing low overall concentrations and molar ratios of $CH_3COOH:NaOH > 1$. All samples exhibit high positive zeta potentials between +34 and +86 mV (Table S8.1), and stable colloidal dispersions are found.

Due to the positive zeta potentials of CAU-55 dispersions, a screening for the adsorption of the anionic dyes was carried out from solution (Figure S9.8).

Anionic organic dye molecules are used in large quantities for example in the textile and paper industries or plastics, but their removal from wastewater remains a challenge.[49,50] A first experiment using CAU-55-HSO_4 and Alizarin Red S (ARS) showed a high adsorption capacity and hence a systematic study using six different anionic dyes was carried out (Figure 5). The adsorption was followed by UV/Vis spectroscopy and fast uptake within minutes is found (Figure 5b). Fixing the amount of dispersed CAU-55-HSO_4 to 1 mmol L^{-1}, the concentration of the dye solution was varied between 0.1 and 5 mmol L^{-1}. Quantitative adsorption of the dye is observed for dye solutions with concentrations under 1 mmol L^{-1} (Figure S9.7). High concentrations of anionic dyes lead to brightly colored composites as shown in Figure 5a and a maximum adsorption capacity of 3.75 $mol_{dye}/mol_{CAU\text{-}55}$ is observed. The adsorption kinetics were evaluated by employing the pseudo-second-order kinetic model to the time-dependent adsorption experiments (section S9.1) leading to a second order kinetic constant (k_2) of 1.1×10^{-3} g min mg^{-1}. Over 80 % dye removal is accomplished within 5 min for CAU-55-HSO_4, which is much shorter than for conventionally used activated carbon[51] or carbon nanotubes[52] (>40 min) and is similar to the adsorption kinetics of some MOFs.[53,54] The adsorption capacity at equilibrium of 239 mg g^{-1} is slightly higher than

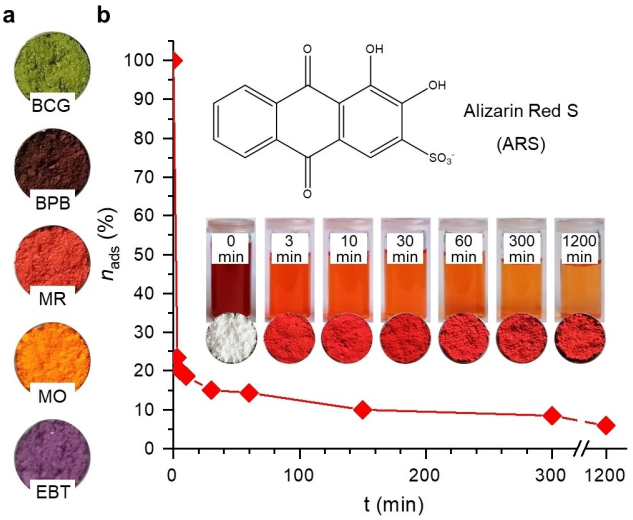

Figure 5. a) CAU-55-HSO_4 powder after the adsorption of anionic dyes (Bromocresol Green (BCG), Bromophenol Blue (BPB), Methyl Red (MR), Methyl Orange (MO) and Eriochrome Black T (EBT)) from solution. b) Fast and effective removal of Alizarin Red S (ARS) from aqueous solution by CAU-55-HSO_4 powder monitored by time-dependent UV/Vis spectroscopy.

for activated carbon materials and in the range of the MOFs Cr-MIL-101 (≈ 115 mg g^{-1})[54] and Fe-MOF-235 (> 400 mg g^{-1}).[53] The adsorption of Methyl Orange (MO) can proceed through coordination to fivefold coordinated Al ions, as recently reported for a Al_{13} derived material.[55] According to the crystal structure determination, the Al^{3+} ions in CAU-55-X are sixfold coordinated and do not have any free coordination sites, which is also confirmed by NMR spectroscopy (Figure S9.3.1–Figure S9.3.4). Electrostatic interactions and hydrogen bonds between the positively charged Al_{24} clusters and the small anions X are found (Figure S3.7) and dye adsorption leads only to small changes in the lattice parameters (Figure S9.2.1–S9.2.3) and influences only a part of the Al atoms (Figure S9.3.3). Therefore, we conclude that mainly electrostatic interactions of the anionic dye and the positively charged particles take place.

Based on the cationic nature of the Al_{24} clusters, preliminary tests for the removal of per- and polyfluoroalkyl substances (PFAS) by CAU-55-HSO_4 were carried out. PFAS are persistent industrial compounds that are of growing environmental and health concerns and often have carboxylate and sulfonate functional groups and are anionic in water at near-neutral pH.[56] Porous materials have been intensively tested for the adsorption and removal of PFAS from groundwater.[57,58] Thus, an aqueous solution containing a mixture of PFAS was treated by stirring in CAU-55-HSO_4 and after 60 minutes CAU-55-HSO_4 was removed by a syringe filter. The removal efficiencies (RE) varied depending on the PFAS species. High REs were achieved for all long-chain perfluorinated PFASs including linear perfluorooctanesulfonic acid (PFOS, 100 % RE), branched PFOS (99.9 % RE), perfluorononanoic acid (PFNA, 85.2 % RE) and perfluorodecanoic acid (PFDA, 98.1 % RE) (Table S10.1, Figure S10.1)).

Conclusion

Systematic high-throughput investigations of the chemical system $AlCl_3/CH_3COOH/NaOH$ led to the discovery of a porous aluminium salt $[Al_{24}(OH)_{56}(CH_3COO)_{12}]Cl_4$ (CAU-55-Cl) containing the Al_{24}-hydroxide-acetate cluster cation $[Al_{24}(OH)_{56}(CH_3COO)_{12}]^{4+}$. The crystal structure of the title compound was elucidated by 3D electron diffraction followed by Rietveld refinement against X-ray diffraction data and further confirmed by DFT geometry optimization. A scalable green synthesis procedure for CAU-55-Cl was developed to the 215 g scale, using cheap, readily available and environmentally benign starting materials and short reaction times. A general synthesis route was developed that allows the incorporation of other anionic species ($X^- = Br^-$, I^-, and HSO_4^-). Relatively high BET surface areas were observed which vary with the anionic counter ion, with a maximum value of 930 $m^2 g^{-1}$. Large water sorption uptakes were also evidenced with a maximum value of 430 $mg g^{-1}$ associated with adsorption in cages and inter-cage voids of the solid. The positive surface charge of the nano- and microcrystalline powders was confirmed by zeta potential measurements and the fast and effective adsorption of anionic dye molecules and adsorption of per- and polyfluoroalkyl substances (PFAS) was demonstrated.

Acknowledgements

Financial support by the state of Schleswig-Holstein and support from the Swedish Foundation for Strategic Research (SSF) is acknowledged. Felix Steinke, Mirjam Poschmann, Niklas Ruser, Jonas Gosch, Lena Liedtke, Michael Chumakovski and the team for spectroscopic measurements of the department of inorganic chemistry (University of Kiel) are thanked for their support with various measurements. In situ PXRD measurements were carried out at P23/PETRAIII at DESY, a member of the Hemholtz Association (HGF). Prof. Lutz Arhens from the Swedish University of Agricultural Sciences is acknowledged for providing the PFAS mixture. The computational work was performed using HPC resources from GENCI-CINES (Grant A0120907613). Open Access funding enabled and organized by Projekt DEAL.

Conflict of Interest

The authors declare no conflict of interest.

Data Availability Statement

The data that support the findings of this study are available in the Supporting Information of this article.

Keywords: Cluster Compound · Electron Diffraction · Green Synthesis · High-Throughput Screening · Microporous Salt

[1] J. Temuujin, T. Jadambaa, K. J. D. Mackenzie, P. Angerer, F. Porte, F. Riley, *Bull. Mater. Sci.* **2000**, *23*, 301–304.
[2] V. S. Mann, O. P. Pandey, *Arabian J. Sci. Eng.* **2021**, *46*, 12445–12463.
[3] N. T. Kyi, K. M. Naing, T. T. Aye, N. Wynn, *J. Myanmar Acad. Arts Sci.* **2005**, *3*, 49–59.
[4] E. T. C. Vogt, B. M. Weckhuysen, *Chem. Soc. Rev.* **2015**, *44*, 7342–7370.
[5] P. Sreenivasulu, D. Nandan, M. Kumar, N. Viswanadham, *J. Mater. Chem. A* **2013**, *1*, 3268.
[6] S. Kowalak, K. J. Balkus, *Collect. Czech. Chem. Commun.* **1992**, *57*, 774–780.
[7] P. Bhanja, J. Na, T. Jing, J. Lin, T. Wakihara, A. Bhaumik, Y. Yamauchi, *Chem. Mater.* **2019**, *31*, 5343–5362.
[8] G. Hu, N. Wang, D. O'Hare, J. Davis, *J. Mater. Chem.* **2007**, *17*, 2257.
[9] A. I. Khan, D. O'Hare, *J. Mater. Chem.* **2002**, *12*, 3191–3198.
[10] Rodiansono, T. Hara, N. Ichikuni, S. Shimazu, *Chem. Lett.* **2012**, *41*, 769–771.
[11] D.-X. Peng, *Ind. Lubr. Tribol.* **2014**, *66*, 124–130.
[12] A. G. Hanssen, M. Langseth, O. S. Hopperstad, *Int. J. Impact Eng.* **2000**, *24*, 475–507.
[13] J. A. Reglero, M. A. Rodríguez-Pérez, E. Solórzano, J. A. de Saja, *Mater. Des.* **2011**, *32*, 907–910.
[14] J. Y. Bottero, D. Tchoubar, J. M. Cases, F. Fiessinger, *J. Phys. Chem.* **1982**, *86*, 3667–3673.
[15] J. Rowsell, L. F. Nazar, *J. Am. Chem. Soc.* **2000**, *122*, 3777–3778.
[16] J. Y. Bottero, J. M. Cases, F. Fiessinger, J. E. Poirier, *J. Phys. Chem.* **1980**, *84*, 2933–2939.
[17] K. L. Shafran, C. C. Perry, *Dalton Trans.* **2005**, 2098.
[18] L. C. W. Baker, J. S. Figgis, *J. Am. Chem. Soc.* **1970**, *92*, 3794–3797.
[19] B. Gu, C. Sun, J. C. Fettinger, W. H. Casey, A. Dikhtiarenko, J. Gascon, K. Koichumanova, K. Babu Sai Sankar Gupta, H. Jan Heeres, S. He, *Chem. Commun.* **2018**, *54*, 4148–4151.
[20] T. Loiseau, C. Volkringer, M. Haouas, F. Taulelle, G. Férey, *C. R. Chim.* **2015**, *18*, 1350–1369.
[21] H. Reinsch, B. Marszałek, J. Wack, J. Senker, B. Gil, N. Stock, *Chem. Commun.* **2012**, *48*, 9486.
[22] H. Reinsch, M. Feyand, T. Ahnfeldt, N. Stock, *Dalton Trans.* **2012**, *41*, 4164.
[23] T. Ahnfeldt, N. Guillou, D. Gunzelmann, I. Margiolaki, T. Loiseau, G. Férey, J. Senker, N. Stock, *Angew. Chem. Int. Ed.* **2009**, *48*, 5163–5166.
[24] W. Zhou, N. Ogiwara, Z. Weng, N. Tamai, C. Zhao, L.-K. Yan, S. Uchida, *Chem. Commun.* **2021**, *57*, 8893–8896.
[25] G. Xing, T. Yan, S. Das, T. Ben, S. Qiu, *Angew. Chem. Int. Ed.* **2018**, *57*, 5345–5349.
[26] S. Yu, G. Xing, L. Chen, T. Ben, B. Su, *Adv. Mater.* **2020**, *32*, 2003270.
[27] S. Ilic, A. M. May, P. M. Usov, H. D. Cornell, B. Gibbons, P. Celis-Salazar, D. R. Cairnie, J. Alatis, C. Slebodnick, A. J. Morris, *Inorg. Chem.* **2022**, *61*, 6604–6611.
[28] A. J. Gosselin, G. E. Decker, A. M. Antonio, G. R. Lorzing, G. P. A. Yap, E. D. Bloch, *J. Am. Chem. Soc.* **2020**, *142*, 9594–9598.
[29] E. Sánchez-González, M. Y. Tsang, J. Troyano, G. A. Craig, S. Furukawa, *Chem. Soc. Rev.* **2022**, *51*, 4876–4889.
[30] A. J. Gosselin, A. M. Antonio, K. J. Korman, M. M. Deegan, G. P. A. Yap, E. D. Bloch, *J. Am. Chem. Soc.* **2021**, *143*, 14956–14961.
[31] W. J. Robinson, *Med. Rec.* **1896**, *50*, 646.
[32] D. Anthony-Langsdale, *J. Text. Inst. Proc.* **1924**, *15*, P598–P602.

[33] C. T. Mortimer, P. W. Sellers, *J. Chem. Soc. Resumed* **1963**, 1978.
[34] P. K. Panda, S. Ramakrishna, *J. Mater. Sci.* **2007**, *42*, 2189–2193.
[35] Y. Eren, D. Akyil, A. Özkara, *Celal Bayar University Journal of Science* **2017**, *13*, 919–923.
[36] T. Sato, S. Ikoma, F. Ozawa, *Thermochim. Acta* **1984**, *75*, 129–137.
[37] N. Stock, *Microporous Mesoporous Mater.* **2010**, 9.
[38] "Poröse, Kristalline Verbindung": B. Achenbach, N. Stock, E. Svensson Grape, A. K. Inge, DE 10,022,106,916, **2022**.
[39] Deposition Numbers 2219079 (for CAU-55-Cl, 3DED), 2219080 (for CAU-55-Br, 3DED), 2219081 (for CAU-55-I, 3DED) and 2226324 (for CAU-55-Cl, Rietveld Refinement) contain the supplementary crystallographic data for this paper. These data are provided free of charge by the joint Cambridge Crystallographic Data Centre and Fachinformationszentrum Karlsruhe Access Structures service. In addition, the raw dataset consisting of several hundred diffraction frames in XDS format, is available in the Zenodo repository, along with a video showing the diffraction frames in quick succession (https://doi.org/10.5281/zenodo.7680724).
[40] M. Benzaqui, R. S. Pillai, A. Sabetghadam, V. Benoit, P. Normand, J. Marrot, N. Menguy, D. Montero, W. Shepard, A. Tissot, C. Martineau-Corcos, C. Sicard, M. Mihaylov, F. Carn, I. Beurroies, P. L. Llewellyn, G. De Weireld, K. Hadjiivanov, J. Gascon, F. Kapteijn, G. Maurin, N. Steunou, C. Serre, *Chem. Mater.* **2017**, *29*, 10326–10338.
[41] T. Loiseau, L. Lecroq, C. Volkringer, J. Marrot, G. Férey, M. Haouas, F. Taulelle, S. Bourrelly, P. L. Llewellyn, M. Latroche, *J. Am. Chem. Soc.* **2006**, *128*, 10223–10230.
[42] C. Volkringer, D. Popov, T. Loiseau, G. Férey, M. Burghammer, C. Riekel, M. Haouas, F. Taulelle, *Chem. Mater.* **2009**, *21*, 5695–5697.
[43] G. Férey, C. Serre, C. Mellot-Draznieks, F. Millange, S. Surblé, J. Dutour, I. Margiolaki, *Angew. Chem. Int. Ed.* **2004**, *43*, 6296–6301.
[44] P. Serra-Crespo, E. V. Ramos-Fernandez, J. Gascon, F. Kapteijn, *Chem. Mater.* **2011**, *23*, 2565–2572.
[45] G. Férey, C. Mellot-Draznieks, C. Serre, F. Millange, J. Dutour, S. Surblé, I. Margiolaki, *Science* **2005**, *309*, 2040–2042.
[46] Y.-J. Liu, Y.-F. Sun, S.-H. Shen, S.-T. Wang, Z.-H. Liu, W.-H. Fang, D. S. Wright, J. Zhang, *Nat. Commun.* **2022**, *13*, 6632.
[47] H. Xu, Y. Wu, L. Yang, Y. Rao, J. Wang, S. Peng, Q. Li, *Angew. Chem. Int. Ed.* **2022**, *61*, e202217864.
[48] R. Stäglich, T. W. Kemnitzer, M. C. Harder, A. Schmutzler, M. Meinhart, C. D. Keenan, E. A. Rössler, J. Senker, *J. Phys. Chem. A* **2022**, *126*, 2578–2589.
[49] V. K. Garg, R. Gupta, A. Bala Yadav, R. Kumar, *Bioresour. Technol.* **2003**, *89*, 121–124.
[50] M. T. Yagub, T. K. Sen, S. Afroze, H. M. Ang, *Adv. Colloid Interface Sci.* **2014**, *209*, 172–184.
[51] S. Chen, J. Zhang, C. Zhang, Q. Yue, Y. Li, C. Li, *Desalination* **2010**, *252*, 149–156.
[52] F. M. Machado, S. A. Carmalin, E. C. Lima, S. L. P. Dias, L. D. T. Prola, C. Saucier, I. M. Jauris, I. Zanella, S. B. Fagan, *J. Phys. Chem. C* **2016**, *120*, 18296–18306.
[53] E. Haque, J. W. Jun, S. H. Jhung, *J. Hazard. Mater.* **2011**, *185*, 507–511.
[54] E. Haque, J. E. Lee, I. T. Jang, Y. K. Hwang, J.-S. Chang, J. Jegal, S. H. Jhung, *J. Hazard. Mater.* **2010**, *181*, 535–542.
[55] Y. Kinoshita, Y. Shimoyama, Y. Masui, Y. Kawahara, K. Arai, T. Motohashi, Y. Noda, S. Uchida, *Langmuir* **2020**, *36*, 6277–6285.
[56] K. H. Kucharzyk, R. Darlington, M. Benotti, R. Deeb, E. Hawley, *Glob. Trends Environ. Remediat. Ind.* **2017**, *204*, 757–764.
[57] R. Li, S. Alomari, R. Stanton, M. C. Wasson, T. Islamoglu, O. K. Farha, T. M. Holsen, S. M. Thagard, D. J. Trivedi, M. Wriedt, *Chem. Mater.* **2021**, *33*, 3276–3285.
[58] R. Li, S. Alomari, T. Islamoglu, O. K. Farha, S. Fernando, S. M. Thagard, T. M. Holsen, M. Wriedt, *Environ. Sci. Technol.* **2021**, *55*, 15162–15171.

Manuscript received: December 17, 2022
Accepted manuscript online: April 27, 2023
Version of record online: June 7, 2023